Nuclear Engineering and Technology xxx (xxxx) xxx

Contents lists available at ScienceDirect

Nuclear Engineering and Technology

journal homepage: www.elsevier.com/locate/net

Original Article

Segmented mandrel tests of as-received and hydrogenated WWER fuel cladding tubes

Márton Király [a, *], Márta Horváth [a], Richárd Nagy [a, b], Nóra Vér [a], Zoltán Hózer [a]

[a] Centre for Energy Research, Budapest, Konkoly-Thege Miklós road 29-33, Hungary
[b] Óbuda University, Doctoral School on Material Sciences and Technologies, Budapest, Bécsi road 96/b, Hungary

ARTICLE INFO

Article history:
Received 6 August 2020
Received in revised form
19 March 2021
Accepted 21 March 2021
Available online xxx

Keywords:
Ductility
Cladding
Hydrogenation
WWER
Nuclear fuel
Mandrel
FEM

ABSTRACT

The mechanical interaction between the fuel pellet and the cladding tube of a nuclear fuel rod is a very important for safety studies as this phenomenon could lead to fuel failure and release of radioactivity. To investigate the ductility of cladding tubes used in WWER type nuclear power plants, several mandrel tests were performed in the Centre for Energy Research (EK). This modified mandrel test was used to model the mechanical interaction between the fuel pellet and the cladding using a segmented tool. The tests were conducted at room temperature and at 300 °C with inactive as-received and hydrogenated cladding ring samples. The results show a gradual decrease in ductility as the hydrogen content increases, the ductile-brittle transition was seen above 1500 ppm hydrogen absorbed.

1. Introduction

During the operation of the nuclear power plant, the fuel pellet undergoes several processes, fragmentation, compacting and swelling, while the cladding creeps inwards towards the pellet due to high external pressure. The coefficients of thermal expansion and the operating temperature of the two materials are also different, so their thermal expansion will also be different during operation. In nuclear power plants, usually within a year or two, the gap between the fuel pellet and the cladding completely closes due to the creep-down of the cladding and the swelling of the fuel. When the pellet and the cladding come into contact, mechanical and chemical interactions occur. The mechanical stress exerted by the pellet can lead to stress corrosion cracking, and together with the iodine formed during fission and released from the pellet, the propagation of the crack in the zirconium can be facilitated by the zirconium iodide that forms in the crack tip. Hydrogen generated during cladding corrosion and water radiolysis also has a negative impact on zirconium ductility at concentrations above 600 ppm [1]. As a result, rapid changes in power can cause the cladding to rupture and fission products to escape into the primary circuit. Therefore, examination of the ductility of the fuel claddings as well as the cracking and fracture behaviour is important both for normal operation and accident scenarios.

During a reactivity-initiated accident (RIA) considered in nuclear power plant safety analyses, the power increases suddenly due to a large reactivity increase in the reactor. The fuel pellet heats up quickly and interacts with the cladding due to its thermal expansion. In WWER fuel, the outer diameter of the fuel pellet, measured at the beginning of operation at room temperature, is 7.6 mm and the inner diameter of the cladding is 7.8 mm. For the sake of argument, if a solid pellet of 7.8 mm outer diameter is heated uniformly from room temperature to 2800 °C near its melting point, the linear expansion is around 4.5% [2], the outer diameter will be 8.15 mm. This value would not be reached by a fuel even in a reactivity accident, but it gives a conservative estimate of the magnitude of the pellet's size change.

In the event of a reactivity accident, the heating and thermal expansion of the fuel pellets takes place in a few milliseconds [3], but the cladding material needs time to heat up. This first phase is called pellet-cladding mechanical interaction (PCMI). Rupture of the cladding can occur in this phase if the thermal expansion is significant and the cladding material is brittle. During a RIA, brittle

* Corresponding author.
E-mail address: kiraly.marton@ek-cer.hu (M. Király).

https://doi.org/10.1016/j.net.2021.03.019

claddings might fail in the elastic range whereas ductile materials are expected to resist after significant plastic deformation induced by the sudden increase of mechanical stress. Similarly, it is important to investigate the long-term behaviour of irradiated claddings exposed to corrosion and hydrogen uptake in normal operation and in an interim dry storage facility. During normal operation, the hydrides are typically oriented in the circumferential direction. The hydrogen can dissolve back into the metal at when the temperature increases, for example, at the initial high temperature drying of the cladding. During dry storage, the internal pressure of the rod slowly decreases as the temperature of the cladding decreases, and the hydrogen can precipitate from the metal into radially oriented hydrides. This can promote crack nucleation and propagation, and the consequences can be important during transportation of the fuel to a final storage facility.

To model the mechanical interaction between the pellet and the cladding (PCMI), tests are often performed using a multi-element tensile tools to determine the ductility limit of the cladding tubes or the rings cut from them. These tools are called segmented expanding mandrels in the literature. Their role is to distribute the radial load evenly along the inner surface of the tubes. The purpose of the test is not to determine the yield or the tensile strength, but to determine the ductile-brittle transition under PCMI conditions.

The advantage of this test is that it is relatively easy to perform, does not require lengthy preparation and reproduces rather well the type of loading expected during PCMI. The initial heat treatment and corrosion of the specimens and the amount of hydrogen and iodine absorbed by them can be controlled, and the test specimen can be inactive or irradiated. It must be noted that in a nuclear reactor the neutron irradiation hardening of the cladding material decreases the ductile-to-brittle transition parameters. These tests can be performed both at room temperature and near the cladding operating temperature (around 350 °C). An important parameter during the measurement can be the composition of the gaseous environment surrounding the sample, especially the amount of iodine and oxygen, which can promote crack propagation.

Unfortunately, mandrel tests are not easily comparable to the widespread ring compression ductility tests as the stresses are fundamentally different in the cladding samples during the two types of tests, the first one being governed by uniform hoop stresses across the cladding and the second rather governed by bending [4]. Using ring compression ductility tests, the ductile-brittle transition was found at a hydrogen content of around 2000 ppm [5].

2. Mandrel testing methods

Before the mandrel tests, the design of the tools and the measurement arrangement may be optimized to achieve the best possible test conditions. In the simplest case, a tools of 4 or up to 12 segments can be used for the tests; the more segments result in a more even stress distribution. Their number is limited only by the means of fabrication. Because these must be inserted inside a tube or a ring with an internal diameter of between 7.5 mm and 9.8 mm (depending on the type of cladding), the mandrels are also extremely small, and consequently small tolerances must be applied in their manufacture. The material of the tool may be steel or some hard ceramic (e.g. tungsten carbide), and may be in direct or indirect contact with the inner surface of the tubular sample. In indirect contact a brittle ring made of alumina ceramic is placed between the tool and the sample which breaks in several places during the measurement to simulate the fragmentation of fuel pellet. The maximum stress is formed at the locations where the edges of the pieces of ceramic are in contact with the cladding, which usually initiates cracks in the sample. If the mandrels are also made of alumina, they can also crack and break during the test [6], i.e. new mandrels are required for each measurement.

There are several other methods to produce the radial compressive force. In one case, a cylinder made of a soft metal (zirconium or aluminium) is compressed inside the tool [6–8], which is deformed so that its diameter increases, thereby transferring the radial load to the tool.

The rate of deformation can be a parameter of interest to test the material. In experiments with a soft metal cylinder, the compression of the core is very slow, typically 0.01 mm/min, which results in significantly slower deformation than in ring tensile tests commonly performed at the rate of 5–50 mm/min. The crack propagation occurs slowly and can be better examined this way, especially in the so-called ramp-and-hold tests with increasing and then constant load, however, the phenomenon of PCMI during a RIA can be orders of magnitude faster.

A good example of the measurement method described above is the mandrel experiments performed in the III. phase of the OECD-coordinated Studsvik Cladding Integrity Program (SCIP). The effect of an expanding pellet during slow power increase and a minor reactivity failure has been studied, particularly the effect of the concentration of oxygen and iodine on the failure mechanism (iodine-induced stress corrosion cracking) [9,10]. During the measurement, an incised ceramic ring simulating the fuel pellet was driven apart by a metal mandrel made of zirconium, and in the middle of the device the spike was moved by a piston (Fig. 1, left side). The stress was concentrated at the edge of the ceramic ring as it pressed against the cladding at an angle driven by the spike, loading the wall of the tube unevenly. The elongation rate of 12.6%/hour simulated the elongation of the cladding that occurs during thermal expansion of the fuel due to a power increase. The rate of 0.36%/hour corresponded to the elongation of the cladding due to the subsequent slow swelling of the pellet and the increased internal pressure.

In a different method developed by Karl- Fredrik Nilsson et al. in JRC-IET Petten [11–13], a conical spike is pressed into the centre of the steel mandrel tools (Fig. 1, right side). The advantage of this method is that the spike and the mandrel are not deformed, so that the transmitted force depends only on the applied force, the cone angle of the spike and the friction between the tools. The radial force on the sample can be determined rather precisely. The stress on the cladding wall is more even with radial and tangential tensile regions. This measurement can be fitted on a regular universal testing machine and the rate of deformation can be controlled accordingly. One of the disadvantages is that the geometry of the tool is more complicated as inner side of the small mandrel tools is also conical.

3. Finite element modelling of the segmented tool

In order to prepare experiments in the Centre for Energy Research (CER, formerly KFKI AEKI or MTA EK) with segmented tools, feasibility and sensitivity analyses were performed using three-dimensional finite element numerical model calculations. The design basis was chosen to be the geometry used by Karl-Fredrik Nilsson et al. in JRC-IET Petten, and 8 mm long E110 cladding ring samples with an outer diameter of 9.1 mm and an average wall thickness of 0.65 mm were to be tested. The finite element modelling of the mandrels was performed using the MSC.Marc-Mentat 2005r3 software package [14]. During the preliminary modelling, the authors only wanted to make an estimate of the stresses in the cladding under the influence of the tools with different symmetries. In this method the inner side of the mandrel is conical and the compressive force is provided by a spike with a

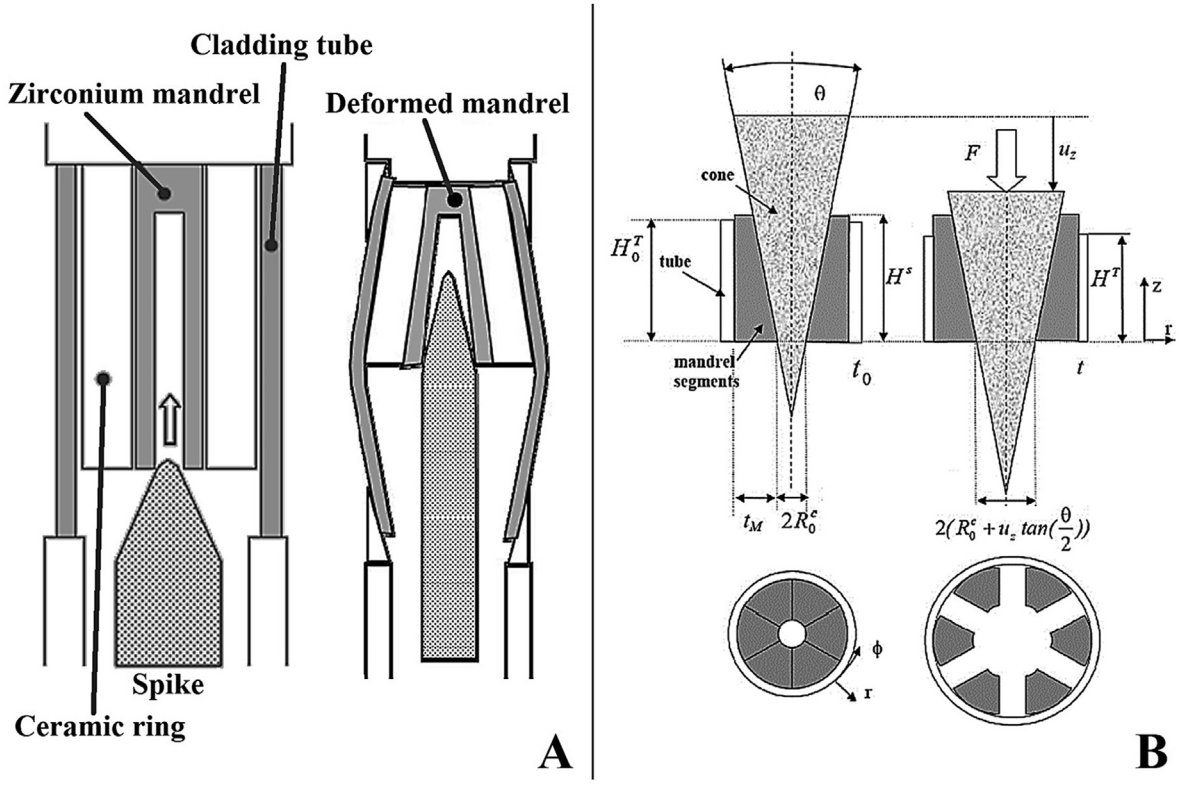

Fig. 1. The sketch of the SCIP mandrel test [9] (A) and the geometry of the mandrels used by Nilsson et al. [12] (B).

given conical angle. The stress concentration was expected at the edges of the mandrels for all measurements. Three cases were investigated, tools with 4, 6 and 8 segments. After the first experiments with the finalized mandrel design, a more detailed dynamic finite element model was developed [15].

The cone angle of the spike has a direct influence on the transmitted displacement rate. When choosing the cone angle of the spike, the possible speed of the crosshead of the universal testing machine was taken into account. Large angles transmit large displacement rates. The 20° cone angle of the original geometry was found to be ill-suited for our measurement. In the case of a large-angle cone, even a small displacement results in a rapid load increase and the minimum speed of the crosshead limits the lowest value of loading rate achievable. Consequently, slow phenomena such as crack propagation and stress corrosion could not be investigated using excessively large angles for the cone angle. Therefore, in the numerical analysis, two additional cases were examined, where the cone angle of the spike was either 20° or 11.4° (chosen for the ease of calculation, as $\sin(5.7°) \approx 0.1$).

After performing the calculations, the values of the obtained equivalent von Mises stresses and the uniformity of the stresses was compared. The stress field in the cladding sample varied according to the number of segments that make up the tool and the size of the gap between the segments. As the number of segments increased, the load acting on the ring samples became more uniform. However, the increase in the number of segments decreases their thickness, this may limit the potential lifetime of the tools. The results of the preliminary numerical simulation confirmed that although increasing the number of mandrels is advantageous, a relatively homogeneous stress field is obtained on the ring samples in each case.

The colour scale of Fig. 2 shows that in the case of a large-angle cone, the stress at the edges of the mandrels increases greatly, which is an order of magnitude smaller for the smaller cone angle. For 8 mm long rings, the wall thickness of the tool at the top of the mandrels would be very small and both this part of the mandrel and the edges in contact with the cone could be deformed. Therefore, the larger cone angle was discarded from further planning.

4. The designed segmented mandrel tool

The segmented expending mandrel tool to be designed for the measurement was based on the results of the preliminary finite element simulation. Due to the small size of the tools and the available manufacturing accuracy (according to ISO2768m, the tolerance is less than 0.1 mm, which can be critical primarily on the inside of the tool), a six-segment tool and a spike with the angle of 11.4° was chosen. Several changes were made to extend the lifetime of the tools and to ease the execution of the measurement.

The height of the active region of the mandrels was determined to be 9 mm. This provides some margins to test rings slightly longer than 8 mm. The radius of the tool was chosen to be 3.7 mm to facilitate the insertion of the ring on the mandrels as burrs may form when the cladding tubes are cut with a lathe, and oxide layer formed on the inner surface of oxidized samples can also reduce the inner diameter of the ring samples. This difference in radius accounts for slight bending of the ring sample at the beginning of the test at the diameter increase of less than 1%, in the elastic phase.

Significant changes were applied to the design of the spike. Based on the finite element simulation, the fit between a conical mandrel and a conical spike with a given upper and lower curvature is not perfect. At the beginning of the test, the cone fits the cavity formed by the mandrels, however, as the measurement progresses and the cone moves downward, the local radius of the cone becomes larger that the local radius of the mandrels, so only the edge

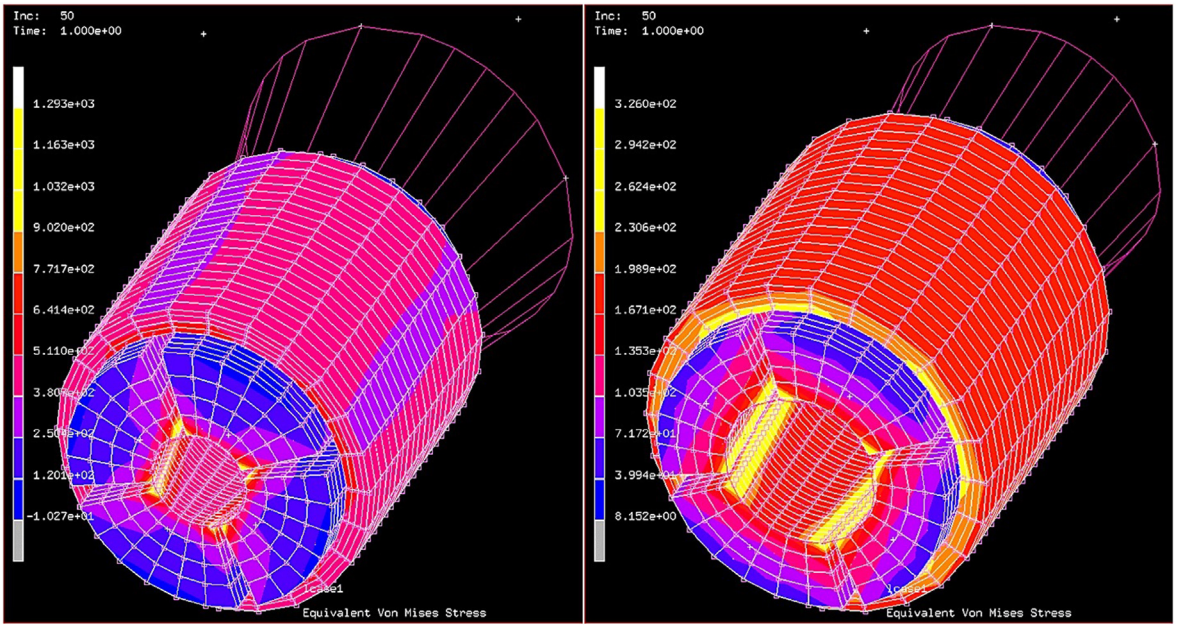

Fig. 2. Results of the preliminary finite element sensitivity study on the influence of the cone angle - mandrel test with 20° (left) and 11.4° cone (right) after 0.1 mm spike displacement, with regards to the equivalent von Mises stresses, viewed from below.

the of the mandrels are in contact with the cone. To eliminate this problem, the conical spike and the mandrels were redesigned into a hexagonal pyramid with planar facets. This allows the plane surfaces of the spike and the mandrels to remain in continuous surface contact during the test. It was expected to improve the accuracy of the data obtained during the measurement and it also simplifies the modelling. This change did not affect the contact between the mandrels and the ring samples, so it didn't affect the distribution of the mechanical load on cladding during tests.

In addition to the active tensile region, a lower, wider part was also added to the mandrels to facilitate the handling of the tool. A ring test piece contacts the upper half of the mandrel, and the lower part forms a solid foundation on which the ring rests at the beginning of the test. As there is negligible axial load on the ring sample, the friction on the bottom of the sample is negligible. This geometric change was also an advantage in the later design phases, as the lower, wider part can also help in removing the spike after the test.

The groove was added on the base of the mandrels that serves to fasten the six mandrels together with a circular spring, which greatly facilitates the assembly and handling of the mandrels in a series of measurements. This allows the multi-piece tool to be held together at the beginning of the test, on which the ring sample can be easily placed, as the radius of the top region is smaller than the inner radius of the cladding. At the end of the test, as the spike moves up, the spring retracts the tools so that the ring can be easily removed and the mandrel segments remain jointly packed. During the measurement, this small spring force does not cause a significant difference in the measured values, and the tool does not fall apart even if the specimen breaks suddenly and violently.

To test the designed tool geometry, mock-up tools were fabricated from alumina (Fig. 3, left side). With the mock-up model, the assembly and handling of the measurement layout was tested, and further improvements were made to the plan. During their assembly, the mock-up mandrels were found to be very small and difficult to handle. For this reason, the base of the tool and the groove holding the spring had to be increased. The maximal radius of the base of the mandrels was determined by the holding tool to be 10.7 mm.

After some practice using the mock-up equipment, the design was finalized (Fig. 3, right side). The tools used for the measurement were manufactured from hardened, heat-treated steel. The mandrels and the spike were made from Böhler K360 ISODUR steel, which cold work tool steel with 8.7% chromium, 2.7% molybdenum and 1.2% vanadium content. Due to the complicated geometry, the production was carried out by CNC-controlled milling. After production, the surfaces were polished to remove the milling marks, and then the tools were hardened by heat treatment at 1050 °C for 20 min to 60 HRC (Rockwell) hardness.

As the friction coefficient strongly affects the force needed to obtain a given displacement, test repeatability and control, it is important to ensure proper lubrication between the contact surfaces. These contacts are between each mandrel and the corresponding side of the pyramidal spike, and between the mandrels and the base. For this reason, it is important to polish the contact surfaces of the tool and the pyramid to reduce their roughness. In the case of room temperature measurements, friction can be minimized with the help of PTFE spray, however, PTFE can no longer be used in the case of high temperature measurements (above 250 °C). It was decided to use the same lubrication regardless of the temperature, a heat-resistant, graphite-based bearing grease was used in all measurements.

5. The holding tool and the furnace

In order to support the mandrels and mount them on a tensile machine, a holding tool or fixture was designed to keep the positioning of mandrels between tests. The measuring arrangement was designed for 3.5 mm radial displacement, i.e., approximately 90% increase in the internal diameter of the rings. This was necessary to reach not just the maximum force, from which the ultimate tensile strength could be calculated, but also the total plastic strain, up to the fracture of the rings. At the maximum displacement the tip of the spike extends below the mandrels, so the holding tool was designed with a hole under the mandrels. The bottom of the holding tool is connected to a load cell located on the lower crosshead of the universal testing machine. The holding tool also helps to separate the mandrels and the spike at the end of the

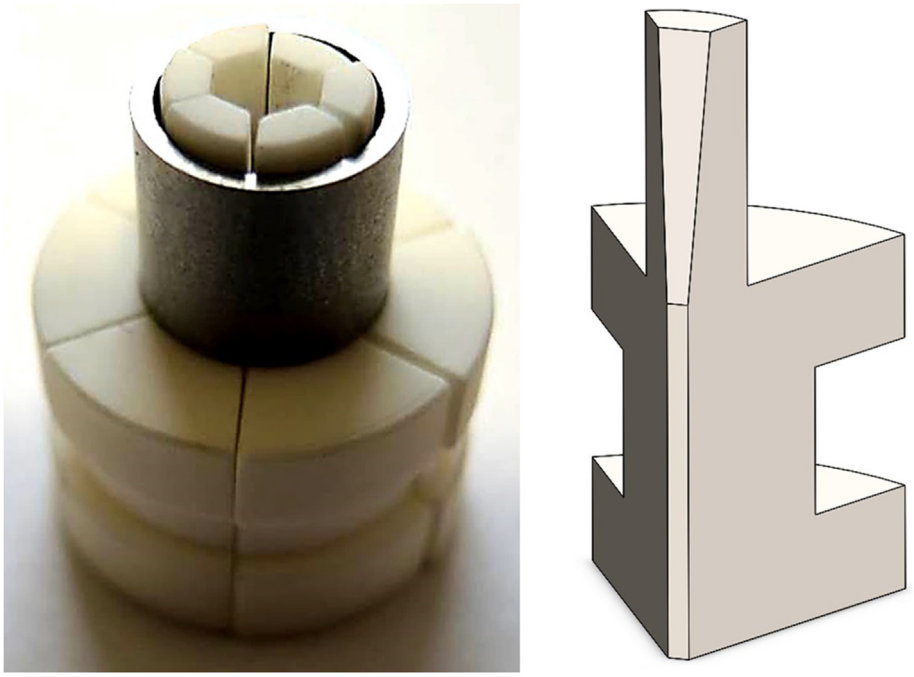

Fig. 3. Mock-up model with an 8 mm cladding ring (left) and the model of the finalized mandrel tool (right).

test. If the test is stopped before the fracture, and ring sample suffered only a small deformation, the spike may become stuck between the mandrels, compressed by the ring, due to the conically interlocking elements. In this case, by lifting the crosshead, the mandrels are pressed against the top plate of the holding tool and the spike can be detached.

A custom tube furnace was designed and built for high temperature measurements. The furnace houses a holding tool designed for mandrels and the extension for the spike. In order to achieve the lowest possible power and heat loss, as well as to ensure rapid heating, the inner diameter was chosen to be 40 mm, which matched the outer diameter of the holding tool. The design basis of the furnace was to be capable to carry out measurements up to 350 °C.

The furnace consists of two parts as seen in Figs. 4 and 5: the upper half heats the spike that is fixed to the crosshead of the universal testing machine with an extension, the lower half heats the ring sample and the holding tool. As the 8 mm rings could only be slid onto the mandrels from above, in order to insert samples to be tested, the furnace has to be opened. The upper half moves independently, while the lower is fixed to the holding tool, the two parts meet in a conical joint when closed. The proper fit between the spike and the mandrels had to be checked each time before closing the furnace.

The furnace keeps the set temperature with an accuracy of ±0.5 °C, and the two sides are controlled separately by two PID controllers and built-in thermocouples. During the first tests it turned out that the controller would overheat the sample. After opening the furnace, the controller would heat at maximum power due to the rapid cooling, but after closing the furnace, the heat loss decreases significantly and the temperature overshoots the set value. To prevent this, the controllers needed to be switched off for a minute, after which they automatically reactivated. This was necessary due to the coupled nature of the two systems, as the lower half of the furnace is in contact with the upper half when closed, however, the masses of the two halves are different. The time between the two measurements, together with the holding time at the set temperature, could be reduced to 10 min.

6. Experimental design

In the current series of measurements, we planned several different tests at EK, which were performed with both E110 cladding made from traditional iodide-electrolytic base metal and the new material from sponge base and with a higher iron content, the E110opt alloy (sometimes called E110G). The material compositions can be found in previous publications [16]. In addition to the as-received samples, the measurement of hydrogenated samples was also planned. The mandrel tests were carried out at room temperature and also at 300 °C. The influence of the loading rate was evaluated using as-received samples at room temperature. In the present study only non-irradiated specimens were tested, for this reason the consequences of irradiation could not be evaluated. However, the results of the present experimental series can be used to explore the effects of oxidation, hydrogen uptake and thermal treatment separately.

Hydrogenation of cladding samples was performed at 600 °C. The hydrogen charging device consisted of a gas inlet system and a high temperature tube furnace combined with a vacuum system. The 8 mm long cladding rings were degreased with an organic solvent (acetone) and then air dried. The samples were weighed on a Mettler Toledo XS205 type analytical balance. The rings (3 + 1 pieces at a time) were first placed in the cold part of the quartz tube outside the furnace on a quartz sample holder with an iron core. After several evacuations, the system was charged with high purity (99.999%) hydrogen to the planned initial pressure, and then the system was pressurized with high purity (99.999%) argon to atmospheric pressure. The sample holder was inserted into the furnace preheated to 600 °C using a strong magnet. The system pressure (hydrogen + argon) was measured and recorded continuously. The pressure drop stopped as the hydrogen absorbed in the samples was in equilibrium with the hydrogen in the gas phase, this process takes approximately 22 h. The amount of hydrogen absorbed was checked by repeated mass measurements. The increase in mass caused by the oxidation due to a very small amount of air and water vapour entering the equipment could be inferred from the measurement of the mass of the heat-treated samples

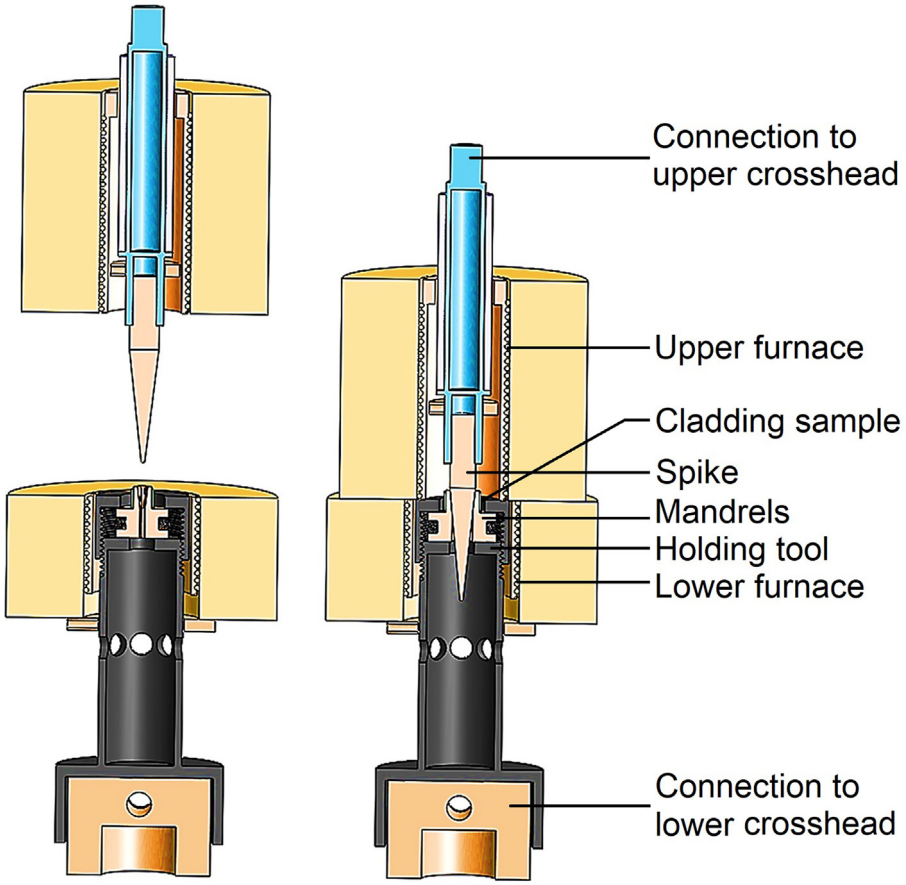

Fig. 4. Cutaway view of the CAD model of the mandrel test with the holding tool and the furnace in opened (left) and closed state (right).

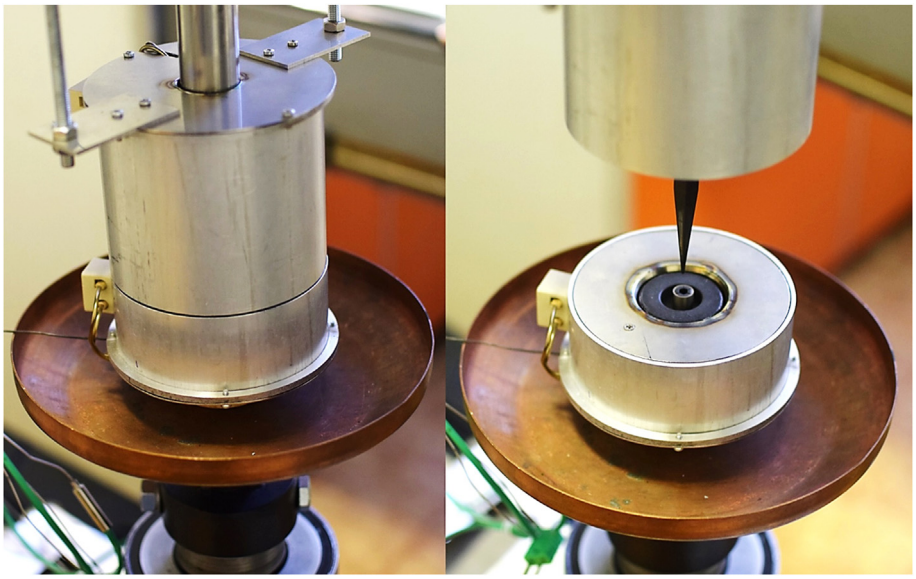

Fig. 5. The furnace in closed (left) and opened state (right) during the mandrel test.

kept in argon without hydrogen, and the data of the samples was corrected. To further reduce this contamination, only the first 3 rings were used for the measurements, the fourth, outermost ring was the "protective" ring that absorbed most of the oxidizing agents. The hydrogen content of a few samples was checked with a ELTRA Oxygen–Hydrogen Analyzer Elementrac OH-p 2 hot extraction device and the accuracy of the mass-based measurements was verified to be over 95%.

7. Experimental

The mandrel tests were performed on an Instron 1195 universal testing machine. Initially there is a gap of about 0.4 mm between the sample ring and the mandrels to facilitate sample placement. At the beginning of the test, the spike attached to the moving crosshead automatically pulls the mandrels into the position of the central axis of the spike, at which point the ring is positioned so that it rests evenly on the tools. This is usually done at a low force, typically below 1000 N. All tests were continued until sample rupture.

The bearing grease Molykote-41 can be used as a lubricating grease at 290 °C or above according to the manufacturer. It is a mixture of phenyl-methyl-silicone and graphite powder. This grease was used in all of the measurement to lubricate both the bottom of the mandrels and between the mandrels and the spike. The application of lubrication reduced the maximum measured force by about 30% compared to sample loading without lubrication. This suggests that changes in friction between parts of the tool could significantly affect the measurement results.

As the brittle samples tended to break into several pieces and fly apart, the measurements were performed in the closed furnace in all cases, even for room temperature tests. The measurement of brittle samples showed that the tools are heavily stressed while measuring the abruptly breaking samples. No permanent deformation was observed on the hardened steel mandrels, but during one test the upper part of a mandrel was broken. This was taken into account in advance as more than six mandrels were prepared for the measurements in order to be able to replace broken mandrels.

8. Evaluation of data

The purpose of the measurement was to model the mechanical interaction between the cladding and the pellet, i.e. to investigate the mechanical behaviour of the cladding after different treatments. Sample ductility can be evaluated based on several different measured and calculated values using mandrel rest results. The maximum internal diameter reached before rupture/failure of the samples contributes to cladding ductility evaluation. The maximum measured force, which is characteristic of the strength of the samples, can also be examined. This value was typically lower for high-ductility samples than for low-ductility samples. The measured maximum force was normalized, divided by the measured length of the ring samples.

The calculation of the area under the force-displacement curve combines the outcomes of the two previously defined parameters. The measured force is proportional to the work required to deform the sample. Since only the displacement of the upper crosshead of the tensile machine (and the spike attached to it) and the compressive force in the vertical direction were measured during the tests, a test-specific number was created from these values. The beginning of the test (point zero) was associated to a measured force of 1000 N.

The integral of the measured force – crosshead (spike) displacement curve was calculated, converted to the diameter increase of the ring samples and normalized by the length of the rings. Although the diameter of the rings did not increase symmetrically, for simplicity, the average internal diameter calculated from the displacement of the mandrel was used. The resulting value (IW or integral work) is proportional to the sum of the work done on the ring samples and the work of friction. This value is proportional to the deformation energy of the rings, but also includes the sum of the work of friction of the tools. The elastic deformation energy was not separated from the plastic deformation because the end of the elastic deformation could not be defined clearly in some measurements. As the deformation was mostly large, the elastic deformation energy component of the integral work was about 2%. Even in the case of quite brittle samples with high hydrogen content, where the maximum deformation was smaller, the elastic component was estimated to be less than 10%.

$$IW = \frac{2 \sin \alpha}{L_{i,0}} \int_{CD_{i,0}}^{CDi,failure} F_i \; dCD_i$$

where: IW – integral work (mJ/mm).

α – mandrel/spike angle (5.7°)
$L_{i,0}$ – original height of ring sample i (mm)
CD_i – measured crosshead displacement (mm)
F_i – measured force (N)

Each day of testing was started with baseline/reference measurement using an as-received sample to check the reproducibility of the mandrel measurement. During these measurements we noticed that the forces recorded during the testing of the as-received reference rings may differ slightly. This can be explained partly by the wear of the contact surfaces of the tools, as this changes the friction coefficient, which can affect the measured force. Because of this, corrections had to be made in some places during the evaluation. The average error for the measured and calculated data was ±3% for all tests.

9. Tests with as-received samples

To determine the loading rate during the test, our setup was compared with previous tensile tests that were performed on 2 mm wide ring samples. The ring tensile tests using two semi-cylindrical drawing tools were generally performed at a crosshead speed of 0.5 mm/min [17,18]. During mandrel testing, a crosshead speed of 2.5 mm/min would result in a similar deformation rate, however, only 2 mm/min could be set on the tensile machine. To determine the optimal loading rate to be used during the series of measurements, preliminary tests were performed at crosshead/spike movement speeds (loading rate) of 0.5 mm/min, 2 mm/min and 5 mm/min. The results are shown in Table 1.

During these first tests, 8 mm long as-received cladding ring samples were used. The 2 mm/min spike displacement speed provides a slow loading rate, the sample reached the maximum force in about 2–3 min and the tests was completed in 12–15 min for the ductile samples. Both as-received zirconium alloys developed large diameter change associated with large plastic deformation, the rupture occurred at an average internal diameter increase of 60–80%.

The slower loading rates resulted in lower maximum force, however, the tests using 0.5 mm/min speed were discontinued because it would have taken up to 1 h for each test. That would have been impractical because of the large amount of samples to be tested. Measurements made at a rate of 5 mm/min did not differ significantly from the ones using 2 mm/min. It was decided to further test all the samples at 2 mm/min to provide sufficient data (using a 2.5 Hz sampling rate for the tensile device load and displacement measurements) to interpret every test including tests with low-ductility samples failing after a rather short testing duration.

Due to the six-part tool, the sample rings have taken a hexagonal shape due to radial deformation on the areas touching the mandrels and tangential stretching between the mandrels. The deformation deduced from the experiments was similar to that

Table 1
Measured and calculated data of as-received samples tested at 20 °C.

Sample No.	Material	Loading rate (mm/min)	Sample length (mm)	Average inner diameter increase (%)	Normalized maximum force (N/mm)	Integral work (mJ/mm)
E1	E110	5	8.03	63.7	491.2	2108
E2	E110	5	7.83	68.6	478.2	2204
E3	E110	2	8.12	63.1	567.4	2578
E4	E110	2	8.22	65.2	596.2	2625
E5	E110	2	8.25	64.1	602.1	2653
E6	E110	2	8.03	66.7	625.2	2500
Eo1	E110opt	0.5	8.14	73.4	389.6	2110
Eo2	E110opt	0.5	8.02	70.9	397.9	2120
Eo3	E110opt	5	8.03	70.5	447.3	2111
Eo4	E110opt	5	8.15	70.3	466.4	2184
Eo5	E110opt	2	8.01	78.6	528.2	2797
Eo6	E110opt	2	8.18	70.3	549.6	2563
Eo7	E110opt	2	8.09	78.7	542.1	2850
Eo8	E110opt	2	8.04	71.8	562.5	2750

expected from the finite element simulation. In the areas between the mandrels, the height of the rings decreased faster so the samples took on the shape of a “crown”, and then at the end of the test the necking started on one of the sides (Fig. 6). The location of this necking varied between measurements, i.e. there was no significant difference between the mandrels, the sample could crack between any two neighbouring segments. In terms of failure process, the crack mostly nucleated in the middle of the narrowed part in the axial direction, and then two crossing localized shear bands appearing on the sample surface. These bands and more specifically their junction are preferential sites for localized damage nucleation, facilitating crack propagation along these damaged bands and sample failure (Fig. 7, white arrow). The 20% diameter change is very similar to that obtained as a result of the detailed finite element simulation [15].

In the test conducted at 300 °C, lower force and increased total elongation was expected based on previous tensile tests [18]. The measured maximum force at 300 °C was about half of that measured at room temperature, and the maximum diameter increase was on average 15% higher than at room temperature (Table 2). The integral work calculated from these values is on average 56% lower than at room temperature. The mode of failure was similar at both temperatures.

10. Tests with hydrogenated samples

Some tests were performed on hydrogenated samples at room temperature and at 300 °C using both alloys to compare their performance. The results are shown in Tables 3 and 4. The samples with 0 wt ppm tested in this sections were subjected only to the heat treatment of the hydrogen charging process in high purity (99.999%) argon atmosphere at 600 °C for 22 h. The heat treatment only slightly modified the mechanical properties of the materials, the diameter increase and the maximum force was similar and the integral work was 10–15% lower than for the as-received samples.

As expected, the samples showed a decreasing ductility with increasing hydrogen content. The plastic deformation of the low-hydrogen samples was gradually replaced by more brittle fracture of the high-hydrogen samples, rupturing at smaller internal diameters. The 4.5% necessary internal diameter increase calculated for the RIA (from the thermal expansion of a solid pellet of 7.8 mm outer diameter from room temperature to 2800 °C) was exceeded by almost all samples, even the high-hydrogen content samples.

Samples could be divided into two categories based on the type of fracture. Samples showing ductile plastic deformation usually endured more than 30% diameter change, and failure typically began with necking and then cracking of the narrowed region from the inside out. Samples showing brittle failure after initial plastic deformation, on the other hand, ruptured along definite, axial cracks, typically with less diameter change and at greater maximum force. This mode of failure was increasingly common above 1200 ppm hydrogen content. Although these samples showed limited ductile plastic strain, and passed the 4.5% ductility criterion, based on the much smaller ductility and their brittle mode of failure, these samples were considered brittle, as in case of longer cladding tube samples the development of axial cracks would be most likely. The behaviour of two such samples is shown in Fig. 9.

The load on low-ductility samples was significantly (50–100%) higher than for very ductile samples, pointing to significant hardening due to the hydrides (Fig. 8). During the tests, the non-linear contribution to the diameter change versus applied load was recorded associated to plastic deformation above 5% diameter change for low hydrogen content samples and the maximum force

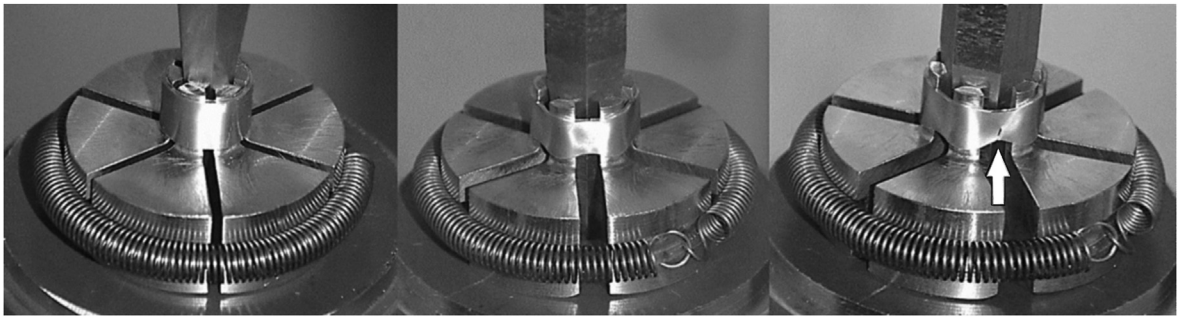

Fig. 6. Stages of sample deformation during the test: Small elastic deformation (left); large plastic deformation, the width and wall thickness of the ring is visibly reduced (middle); ductile crack nucleation just before failure at the centre of a region affected by significant necking (right).

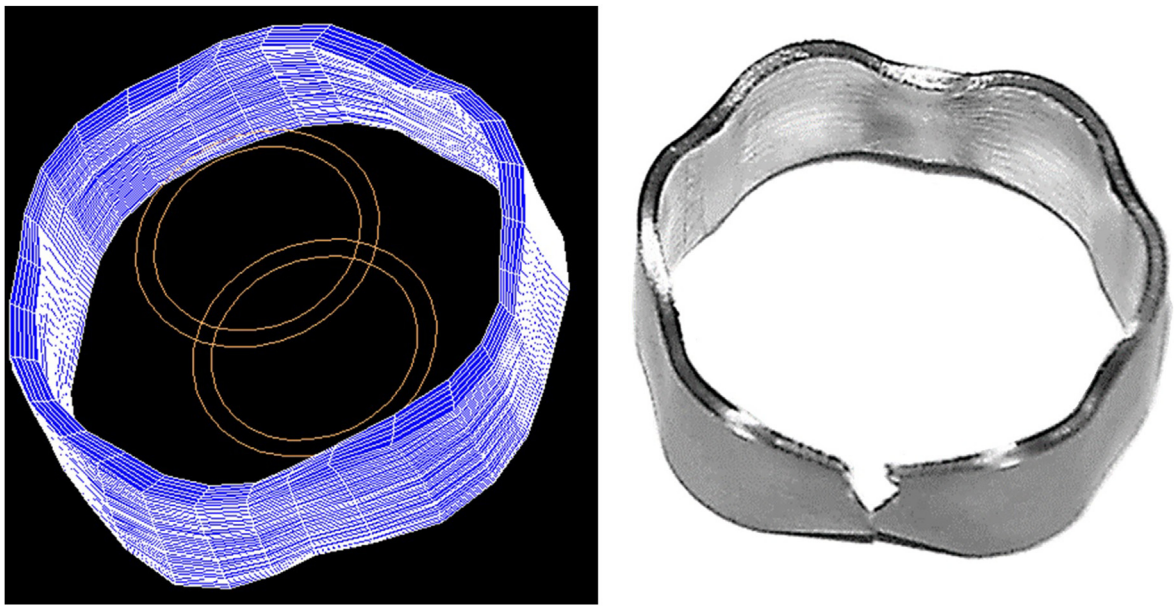

Fig. 7. The calculated (left) and actual shape of an as-received E110 sample after the test (right). The orange circles in the model show the original outline of the cladding ring. (For interpretation of the references to colour in this figure legend, the reader is referred to the Web version of this article.)

Table 2
Measured and calculated data of as-received samples tested at 300 °C.

Sample No.	Material	Loading rate (mm/min)	Sample length (mm)	Average inner diameter increase (%)	Normalized maximum force (N/mm)	Integral work (mJ/mm)
E7	E110	2	8.02	76.9	231.3	1100
E8	E110	2	8.11	77.8	226.7	1069
E9	E110	2	8.11	74.2	248.9	1174
Eo9	E110opt	2	8.01	84.6	243.8	1225
Eo10	E110opt	2	8.15	87.5	246.1	1273
Eo11	E110opt	2	8.18	82.7	256.1	1267
Eo12	E110opt	2	8.09	84.9	254.8	1229

Table 3
Measured and calculated data of hydrogenated samples tested at 20 °C.

Sample No.	Material	Hydrogen content (wt ppm)	Sample length (mm)	Average inner diameter increase (%)	Normalized maximum force (N/mm)	Integral work (mJ/mm)
EH1	E110	0	7.99	69.9	549.9	2383
EH2	E110	0	8.1	65.2	560.8	2175
EH3	E110	313	8.02	57.6	519.5	2017
EH4	E110	737	8.06	48.1	622.9	1702
EH5	E110	1093	7.85	39.9	703.1	1557
EH6	E110	1351	8.14	33.3	772.8	1183
EH7	E110	1555	8.08	22.4	838.8	1193
EH8	E110	2024	8.10	15.3	843.3	1026
EH9	E110	3081	8.10	8.4	797.8	443
EoH1	E110opt	0	8.02	68.9	592.7	2403
EoH2	E110opt	0	8.03	65.1	581.5	2222
EoH3	E110opt	327	8.01	55.6	568.7	2098
EoH4	E110opt	627	8.02	41.5	675.1	1752
EoH5	E110opt	975	8.03	33.2	839.6	1747
EoH6	E110opt	1283	8.06	25.9	924.7	1248
EoH7	E110opt	1563	8.14	21.0	943.5	959
EoH8	E110opt	2059	8.16	12.9	999.7	766
EoH9	E110opt	3026	8.14	7.8	927.2	438

was reached at slightly higher diameter change. In the case of less ductile samples, the measured force continued to increase above this yield strength of the as-received material, and then these samples suddenly broke into several pieces. The maximum force values reach a limit between 1500 and 2000 ppm, after which the maximum force doesn't increase further, this can be considered as the plastic-brittle transition. Although the forces measured for the E110opt were mostly 15–20% higher due to the slightly higher tensile strength than that of the E110, in terms of ductility and embrittlement, there is no significant difference between the two alloys as the average inner diameter increase was similar for both.

If we examine the maximum internal diameter reached during

Table 4
Measured and calculated data of hydrogenated samples tested at 300 °C.

Sample No.	Material	Hydrogen content (wt ppm)	Sample length (mm)	Average inner diameter increase (%)	Normalized maximum force (N/mm)	Integral work (mJ/mm)
EH10	E110	0	8.17	81.2	204.1	1059
EH11	E110	494	8.09	60.7	272.0	1075
EH12	E110	1010	8.11	46.5	325.9	1001
EH13	E110	1501	8.11	36.2	360.6	827
EH14	E110	1989	8.27	23.1	342.2	503
EH15	E110	2486	8.02	19.0	323.6	381
EH16	E110	2523	8.21	19.7	343.6	391
EoH10	E110opt	0	8.07	82.2	204.5	1074
EoH11	E110opt	494	8.15	62.4	283.6	1131
EoH12	E110opt	1009	8.08	49.7	358.3	1121
EoH13	E110opt	1483	8.11	31.9	414.2	874
EoH14	E110opt	1994	8.11	22.8	464.6	666
EoH15	E110opt	2496	8.12	21.6	404.9	503

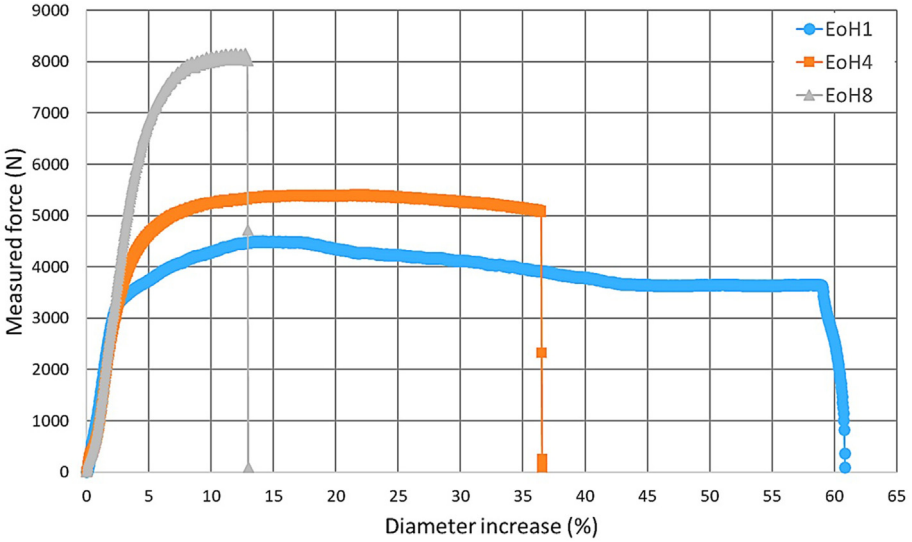

Fig. 8. Force-diameter increase curve of the tests of three samples with different hydrogen content (EoH1 0 ppm; EoH4 627 ppm; EoH8 2059 ppm).

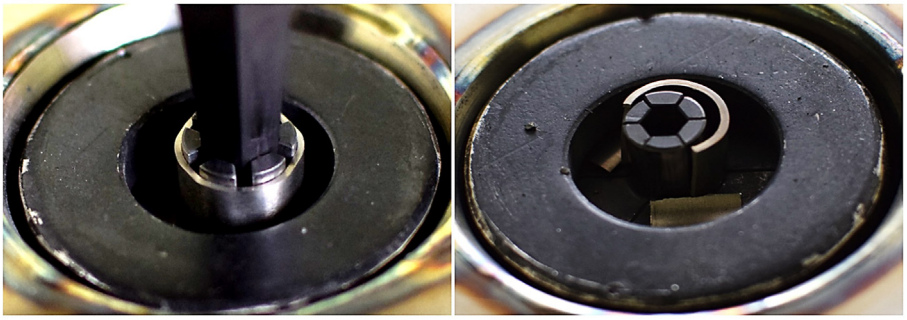

Fig. 9. State of a ductile (EoH4 627 ppm hydrogen, left side) and a brittle (EoH8 2059 ppm hydrogen, right ride) hydrogenated E110opt sample after the same spike displacement.

the measurement, it is clear that by increasing the hydrogen content, the degree of ductility of the rings decreases significantly. The diagrams depicting the important parameters (Figs. 10–12) show similar patterns at the room temperature and at 300 °C. As the hydrogen content increases, the samples rupture at smaller inner diameters. The ductility decreased almost linearly up to the hydrogen content of 2000 ppm, at higher hydrogen content a transition/plateau can be seen.

The diagram depicting the integral work (Fig. 12) shows a difference between room temperature and 300 °C. In the tests conducted at 300 °C, lower force and increased total elongation was expected. However, in contrast to room temperature measurements, the integral work did not decrease up to 1000 ppm hydrogen as the maximum diameter increase exceeded that measured at room temperature. This is partly due to the greater relative scatter of the measured values and partly to the fact that the zirconium alloy rings showed a more plastic behaviour at higher temperatures, i.e. the higher ductility at higher temperatures somewhat compensated for the hardening effect of the hydrogen.

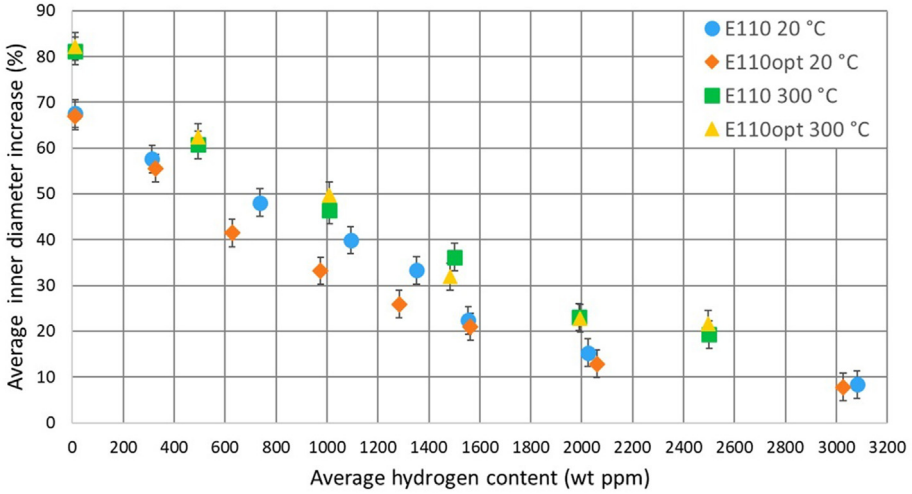

Fig. 10. The average maximum diameter increase before rupture with the hydrogen content of the samples.

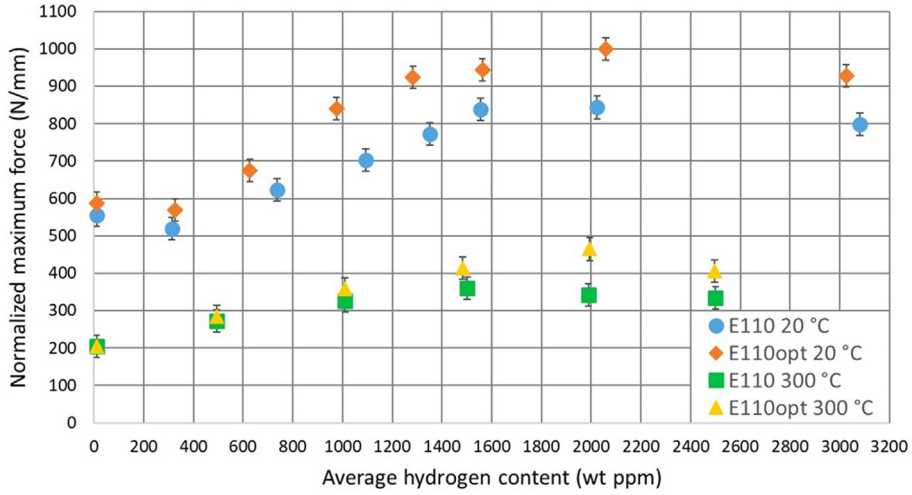

Fig. 11. The normalized maximum force with the hydrogen content of the samples.

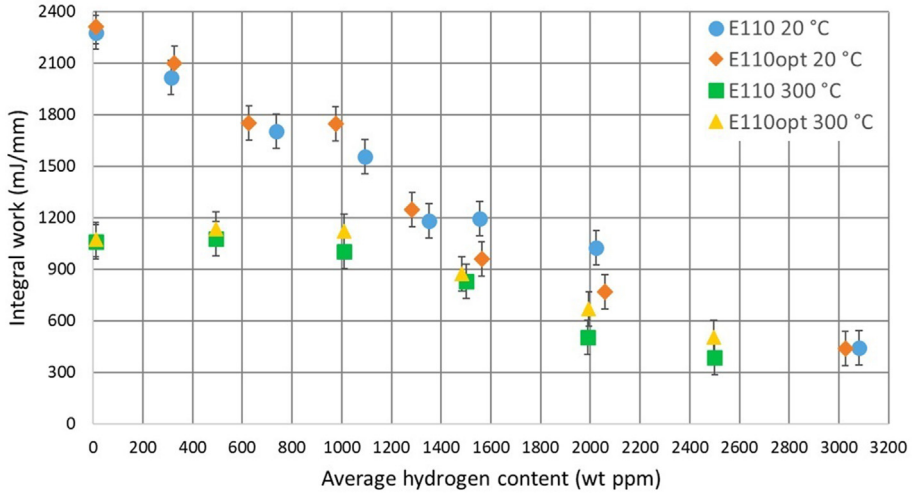

Fig. 12. The integral work with the hydrogen content of the samples.

Overall, the behaviour of the rings does not change significantly after approximately 2000 ppm of absorbed hydrogen at the two temperatures. These brittle samples rupture at 100% higher force and at 80% less diameter increase compared to samples containing little or no hydrogen. The ductility over 2000 ppm hydrogen was 10–20% maximum diameter increase before rupture, depending on the temperature. Technically all could be considered ductile, however, it is important how much plastic margin the samples they had. In addition, an important aspect was that 8 mm long rings that behave differently than full rods. For this reason, the authors have also started designing longer mandrels that load the middle of a longer pipe section. This method will hopefully reproduce the long axial cracks observed in real fuel elements [1] on the less ductile, brittle-failure samples with hydrogen content above 1500 ppm.

Both the segmented mandrel tests and the earlier ring compression tests [5] suggest that the cladding material reaches its minimum ductility at a hydrogen content of around 2000 ppm and can be considered mostly brittle from there. However, the sharp transition found in ring-compression studies between plastic and brittle fracture was not observed, as the more uniform loading of the samples in a segmented mandrel test promotes plastic deformation.

Two more tests performed with hydrogenated “protective” ring samples should be mentioned. According to the mass measurement, they contained 2000–2500 ppm hydrogen, however, due to some air entering the hydrogenation furnace, their surface was slightly blackened (oxide) or yellowed (nitride). This contamination was below 500 ppm based on the blind tests. These rings protected the three real samples from oxidation during hydrogen loading. Some of these samples were mandrel tested and these samples ruptured long before the expected maximum force was reached and showed no plastic deformation at all. The immediate brittle fracture of these rings suggests that in addition to the absorbed hydrogen, even this very mild oxidation/nitridation can significantly impair the plastic behaviour of the claddings.

The detailed finite element modelling of the segmented mandrel tests was performed based on the initial results, published in a separate article [15]. During the FEM analysis, the measured the force-displacement curves were replicated for the samples mentioned in this article. A simple correlation was found between the hydrogen content of the samples and the change in the flow characteristics, a parameter needed for the modelling of less ductile samples.

11. Summary

In this article, a new approach and methodology was presented to simulate the effects of the pellet-cladding mechanical interaction in order to study the effects of different thermal and chemical treatments on the ductility of cladding tubes. This testing method was based on previous segmented mandrel test, however, significant changes were made in both measurement geometry and data evaluation.

To investigate the ductility of cladding tubes used in WWER type nuclear power plants, mandrel tests were performed in the Centre for Energy Research (EK) with inactive pre-treated ring samples modelling the mechanical interaction between the fuel pellet and the cladding. Finite element modelling and concurrent CAD design were used to determine the best suited geometry. A unique segmented mandrel tool was designed and several measurements were carried out at room temperature and at 300 °C on as-received and hydrogenated cladding samples.

The results show a gradual loss in ductility at both temperatures up to a hydrogen content of 2000 ppm, after which the alloys reach minimal ductility. This limit can be considered as the plastic-brittle transition threshold, however, the transition between the two modes of failure is gradual. Although the forces measured for the E110opt were higher due to the higher tensile strength of the as-received tubes compared to E110, in terms of ductility and embrittlement, there was no significant difference between the two alloys.

Declaration of competing interest

The authors declare that they have no known competing financial interests or personal relationships that could have appeared to influence the work reported in this paper.

Acknowledgement

The research activities presented were supported by Paks NPP (contract number: 4000172048. EK-G-1175/2015). The National Research, Development and Innovation Fund of Hungary (contract number: NVKP_16-1-2016-0014) and the European Joint Programme on Radioactive Waste Management (EURAD) Spent Fuel Characterisation and evolution until disposal (SFC) workpackage (EU grant agreement number: 847593). There is no conflict of interest in the funding and the publication of this research.

References

[1] K. Edsinger, J. Davies, R. Adamson, in: G. Sabol, G. Moan (Eds.), Degraded Fuel Cladding Fractography and Fracture Behavior. 12th International Symposium on Zirconium in the Nuclear Industry, ASTM International), West Conshohocken, PA, 2000, pp. 316–339.
[2] Thermophysical Properties Database of Materials for Light Water Reactors and Heavy Water Reactors, IAEA-TECDOC-1496, June 2006, p. 57.
[3] Nuclear Fuel Behaviour under Reactivity-Initiated Accident (RIA) Conditions. State-Of-The-Art Report, Nuclear Energy Agency Committee on the Safety of Nuclear Installations, 2020. OCDE 2010 NEA No. 6847. NEA/CSNI/R(2010)1.
[4] S. Holmström, et al., EERA JPNM Pilot Project TASTE, Test Methodologies for Determining High Temperature Material Properties of Thin Walled Tubes, European Commission Joint Research Centre, 2017 (JRC) Technical report, JRC10558, EUR 28642 EN.
[5] T. Novotny, E. Perez-Feró, M. Horváth, Hydrogenation and high temperature oxidation of Zirconium claddings, in: Proceedings of 11th International Conference on WWER Fuel Performance. Modelling and Experimental Support. Varna, Bulgaria, 26 Sep - 3 Oct 2015, pp. 370–375.
[6] B.N. Nobrega, J.S. King, G.S. Was, S.B. Wisner, Improvements in the design and analysis of the segmented expanding mandrel test, J. Nucl. Mater. 131 (1985) 99–104.
[7] J.P. Foster, Segmented expanding mandrel test methods (Letter to editors), J. Nucl. Mater. 150 (1987) 342–350.
[8] H. Jiang, J.-A.J. Wang, Methodology for mechanical property testing of fuel cladding using an expanding plug wedge test, J. Nucl. Mater. 446 (2014) 27–37.
[9] SCIP III – report, Technical Description. Studsvik Report. STUDSVIK/N-13/172.
[10] M. Dostál, J. Klouzal, M. Valach, P. Magnusson, F. Corleoni, FEM modelling of the expanding mandrel test simulating out-of-pile PCI SCC of fuel cladding, in: Proceedings of 23rd Conference on Structural Mechanics in Reactor Technology (SMiRT-23), Manchester, UK, August 10-14, 2015.
[11] K.-F. Nilsson, C. Chenel-Ramos, V. Vokál, J. Mendes, O. Martin, Development of the Mandrel Test for Controlled Displacement of Zircaloy Tubes, JRC Report, 2008, pp. 1–38. EUR 23283 EN, ISSN: 1018-5593.
[12] K.-F. Nilsson, O. Martin, C. Chenel-Ramos, J. Mendes, The segmented expanding cone-mandrel test revisited as material characterization and component test for fuel claddings, Nucl. Eng. Des. 241 (2011) 445–458.
[13] K.-F. Nilsson, M. Négyesi, Z. Száraz, I. Simonovski, An evaluation of the segmented expanding cone-mandrel test to assess hydride re-orientation and ductility reduction for Zircaloy-2 cladding tubes, J. Nucl. Mater. 466 (2015) 220–233.
[14] MSC.Marc Vol. A: Theory and User Information. Version 2005. MSC Software Corporation Ltd.
[15] R. Nagy, M. Király, D.M. Antók, L. Tatár, Z. Hózer, Dynamic finite element

analysis of segmented mandrel tests of hydrogenated E110 fuel cladding tubes, Mater. Today Commun. 24 (2020) paper 101005.

[16] M. Király, K. Kulacsy, Z. Hózer, E. Perez-Feró, T. Novotny, High-temperature steam oxidation kinetics of the E110G cladding alloy, J. Nucl. Mater. 475 (July 2016) 27–36.

[17] M. Király, D.M. Antók, M. Horváth, Z. Hózer, Evaluation of axial and tangential ultimate tensile strength of zirconium cladding tubes, Nucl. Eng. Technol. 50 (Issue 3) (2018) 425–431.

[18] M. Király, Z. Hózer, M. Horváth, T. Novotny, E. Perez-Feró, N. Vér, Impact of thermal and chemical treatment on the mechanical properties of E110 and E110G cladding tubes, Nucl. Eng. Technol. 51 (Issue 2) (2019) 518–525.